JCTC Journal of Chemical Theory and Computation

Article

pubs.acs.org/JCTC

Graphite and Hexagonal Boron-Nitride have the Same Interlayer Distance. Why?

Oded Hod*

Department of Chemical Physics, School of Chemistry, The Sackler Faculty of Exact Sciences, Tel Aviv University, Tel Aviv 69978, Israel

Supporting Information

ABSTRACT: Graphite and hexagonal boron nitride (*h*-BN) are two prominent members of the family of layered materials possessing a hexagonal lattice structure. While graphite has nonpolar homonuclear C−C intralayer bonds, *h*-BN presents highly polar B−N bonds resulting in different optimal stacking modes of the two materials in the bulk form. Furthermore, the static polarizabilities of the constituent atoms considerably differ from each other, suggesting large differences in the dispersive component of the interlayer bonding. Despite these major differences, both materials present practically identical interlayer distances. To understand this finding, a comparative study of the nature of the interlayer bonding in both materials is presented. A full lattice sum of the interactions between the partially charged atomic centers in *h*-BN results in vanishingly small contributions to the interlayer binding energy. Higher order electrostatic multipoles, exchange, and short-range correlation Kohn−Sham contributions are found to be very similar in both materials and to almost completely cancel out by the kinetic energy term, which partly represents the effects of Pauli repulsions, at physically relevant interlayer distances, resulting in a marginal effective contribution to the interlayer binding. Further analysis of the dispersive energy term reveals that despite the large differences in the individual atomic polarizabilities, the heteroatomic B−N C_6 coefficient is very similar to the homoatomic C−C coefficient in the hexagonal bulk form, resulting in very similar dispersive contribution to the interlayer binding. The overall binding energy curves of both materials are thus very similar, predicting practically the same interlayer distance and very similar binding energies. The conclusions drawn here regarding the role of electrostatic interactions between partially charged atomic centers for the interlayer binding of *h*-BN are of a general nature and are expected to hold true for many other polar layered systems.

I. INTRODUCTION

Layered materials are playing a central role in a variety of key scientific fields, including nanoscale materials science, condensed matter physics, molecular electronics and spintronics, tribology, and chemistry. While their intralayer interactions are often well characterized and dominated by covalent bonding, the interlayer interactions are determined by a delicate balance between dispersion forces, electrostatic interactions, and Pauli repulsions. Understanding the relative contribution of each of these interactions to the interlayer binding is therefore essential for the characterization of their mechanical, electronic, and electromechanical properties and for the design of new materials with desired functionality.[2−8]

In recent years, the most prominent member of the family of layered materials has been graphene,[9−12] which serves as a building block for few-layered graphene and graphite as well as for single- and multi-walled carbon nanotubes.[13] Here, each layer is an atomically thin hexagonal sheet of sp^2 bonded carbon atoms, where the unpaired p_z electrons on each atomic site join to form a collective π system, turning the material into a semimetal. The main factors expected to dominate graphene interlayer binding are electrostatic interactions, dispersive interactions, and Pauli repulsions between the electron densities of each layer. Focusing on electrostatic interactions, the complex electron density profile around each atomic center may be characterized by its deviation from spherical symmetry via its higher-order (beyond the monopole) multipoles.[5] Due to the nonpolar nature of the homonuclear carbon−carbon bond a zero effective charge resides on each atomic center. Thus, the classical interlayer monopole−monopole electronic interactions are completely canceled out by the corresponding nuclear−nuclear electrostatic contributions. This leaves higher order electrostatic multipole interactions, dispersion interactions, and Pauli repulsion as the leading factors governing the stacking and registry of the layered structure.[14−26] Here, the complex interplay between these factors dictates the equilibrium interlayer distance[16] and the optimal AB staking mode (see Figure 1) where consecutive layers are shifted with respect to each other such that half of the carbon atoms of one layer reside above the hexagon centers of the adjacent layers.[7,8]

The inorganic analog of graphene, sometimes referred to as "white graphene",[27−29] is hexagonal boron nitride.[30−40] Structurally, a single layer of *h*-BN is very similar to a graphene sheet having a hexagonal backbone where each couple of bonded carbon atoms is replaced by a boron−nitride pair, making the two materials isoelectronic. Nevertheless, due to the electronegativity differences between the boron and the nitrogen atoms, the π electrons tend to localize around the nitrogen atomic centers,[41−44] thus forming an insulating material. Furthermore, the polarity of the B−N bond results in the buildup of effective charges on the atomic centers, thus allowing for interlayer electrostatic interactions between partially charged atoms to join higher order electrostatic multipole interactions, dispersion

Received: December 8, 2011
Published: January 31, 2012

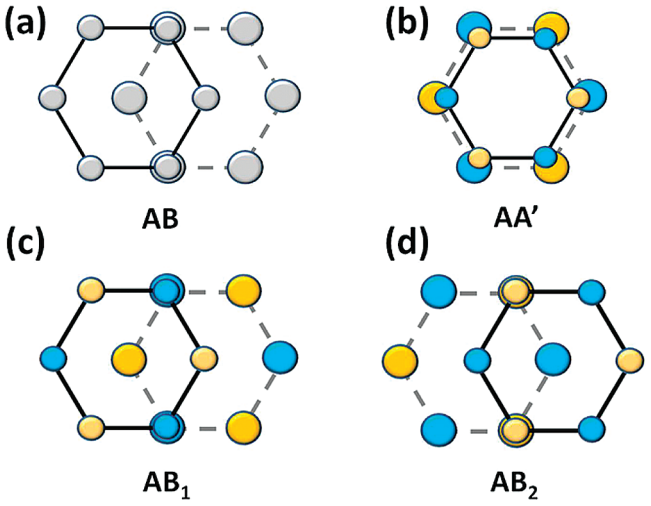

Figure 1. High symmetry stacking modes in hexagonal lattices. (a) The optimal AB stacking of graphite has a carbon atom in a given layer residing atop the center of a hexagon of the adjacent layers. (b) The optimal AA′ stacking mode of *h*-BN has a partially negatively charged nitrogen atom in one layer residing on top of a partially positively charged boron atom in the adjacent layers. This configuration minimizes the electrostatic energy. (c) The metastable AB_1 stacking mode of *h*-BN has eclipsed boron atom positions, whereas the nitrogen atoms appear on top of hexagon centers of adjacent layers. (d) The unstable AB_2 stacking mode of *h*-BN has eclipsed nitrogen atom positions whereas the boron atoms appear on top of hexagon centers of adjacent layers. Lower (upper) layer hexagons are indicated by larger (smaller) circles representing the atoms and dashed (full) lines representing sp^2 covalent bonds. Blue (orange) circles represent boron (nitrogen) atoms. From a naïve electrostatic viewpoint, the AB_1 and AB_2 stacking modes of *h*-BN should be energetically equivalent; however, due to the vanishing electrostatic interactions between partially charged atomic centers on adjacent layers and enhanced Pauli repulsions between eclipsed nitrogen centers, the AB_1 configuration is close in total energy to the AA′ stacking mode, whereas AB_2 is an unstable high energy mode.

interactions, and Pauli repulsion in dictating the nature of the interlayer binding. This, in turn, stabilizes the AA′ stacking mode (see Figure 1) where a boron atom bearing a partial positive charge in one layer resides between the oppositely charged nitrogen atoms on the adjacent layers.

On the basis of the above considerations, one may generally deduce that electrostatic interactions between partially charged atomic centers may play a crucial role in the interlayer binding of polar layered materials.[41] Specifically, the electrostatic attractions between the oppositely charged atomic centers in adjacent *h*-BN layers are expected to result in a considerably shorter interlayer distance than that measured for graphite. Nevertheless, the interlayer distances in graphite (3.33−3.35 Å)[45−47] and *h*-BN (3.30−3.33 Å)[48−53] are essentially the same, suggesting that electrostatic interactions between partially charged atomic centers, which exist in *h*-BN and are absent in graphite, have little effect on the interlayer binding. This is consistent with a recent study showing that van der Waals (vdW) forces, rather than electrostatic interactions, are responsible for anchoring the *h*-BN layers at the appropriate interlayer distance.[8] Further support for this argument is found when comparing the optimal AA′ stacking mode with the AB_1 stacking mode where the partially positively charged boron sites are eclipsed and the nitrogen atoms reside atop hexagon centers in adjacent layers (see Figure 1). From a naïve electrostatic viewpoint, one would expect the AA′ mode, where opposite charges reside atop each other, to be considerably lower in energy than the AB_1 mode, whereas according to advanced *ab initio* calculations, the latter is found to be only 0.875−2.0 meV/atom higher in energy.[8,29,54] Furthermore, when considering the AB_2 stacking mode (see Figure 1), which in terms of electrostatic interactions between partially charged atomic centers is equivalent to the AB_1 mode, its total energy is higher by as much as 6.5−12.0 meV/atom than both the AA′ and the AB_1 modes.[8,54,55] This may be related to enhanced Pauli repulsions between the more delocalized overlapping electron clouds of the nitrogen atoms.[5,29,41,54,56−58]

To add to the puzzle, even if one accepts that electrostatic interactions between partially charged atomic centers do not contribute to the binding in the polar *h*-BN system, the differences in spatial distribution of the charge densities in graphene and *h*-BN would suggest that the contribution of higher order electrostatic multipoles as well as Pauli repulsions would be different in both materials. Furthermore, the large differences in the values of the static polarizabilities of the boron, carbon, and nitrogen atoms suggest that the dispersive contribution to the binding would behave differently in the two materials. Several questions thus arise: Why is the effect of electrostatic interactions between partially charged atomic centers on the interlayer binding of *h*-BN negligible? Why is the effect of higher-order electrostatic multipoles in both graphene and *h*-BN similar? Why is the dispersive attraction similar in both materials? And more generally, is the fact that the interlayer distances of graphite and *h*-BN are so similar a mere coincidence or an effect of a more generic nature? To answer these questions, we present, below, a thorough comparative analysis of the different energy contributions to the interlayer binding in graphene and *h*-BN. We start by explaining why classical electrostatic interactions between partially charged atomic centers have a negligible contribution to the interlayer binding in *h*-BN. This is followed by a comparative study of the classical electrostatic contributions from higher order electrostatic multipoles, nonclassical electrostatic effects, and Pauli repulsions in the two materials, as captured by the electrostatic, exchange and short-range correlation, and kinetic energy terms of standard Kohn−Sham density functional theory approximations. Finally, we compare the long-range interlayer dispersive interactions in both materials.

II. ELECTROSTATIC INTERACTIONS BETWEEN PARTIALLY CHARGED ATOMIC CENTERS

We start by addressing the question regarding the marginal effect of electrostatic interactions between partially charged atomic centers on the binding energy of *h*-BN. Here, the answer lies in the long-range nature of the Coulomb interactions. Our intuition for enhanced electrostatic binding in *h*-BN stems from the attraction of oppositely charged boron and nitrogen atoms residing opposite each other on adjacent layers at the optimal AA′ stacking mode. Nevertheless, the interlayer Coulomb interactions between laterally shifted atomic sites are nonnegligible and must be appropriately taken into account. Specifically, when placing a test charge above a *h*-BN layer, as the lateral distance r from this test charge is increased, the Coulomb interaction decays as $\alpha/(r^2 + h^2)^{1/2}$ which follows α/r as $r \to \infty$, where α is the effective partial charge on each atomic site and h the fixed distance between the charge and the *h*-BN plane. However, the number of atomic sites interacting with the test charge at the given lateral distance r is

dx.doi.org/10.1021/ct200880m | J. Chem. Theory Comput. 2012, 8, 1360−1369

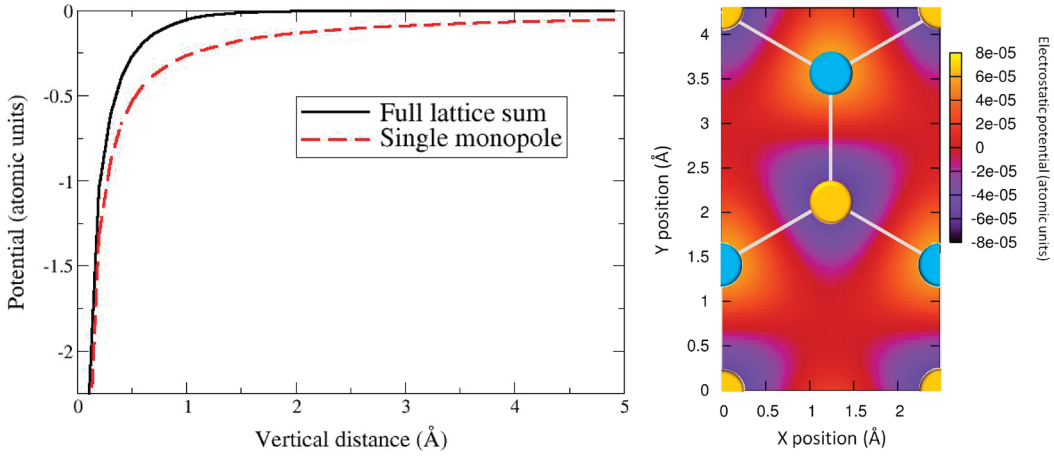

Figure 2. Electrostatic potential (atomic units) due to all partially charged atomic centers above a *h*-BN surface. Left panel: Electrostatic potential above a partially negatively charged ($-0.5e^-$) nitrogen site as a function of the vertical distance from the plane of the *h*-BN layer (solid black curve) calculated using eq 1. For comparison purposes, the potential above a corresponding partially charged isolated nitrogen atom is presented by the dashed red line. Right panel: Full electrostatic potential surface 3.33 Å above the *h*-BN layer calculated using eq 1. Boron (nitrogen) atomic positions are represented by blue (orange) circles. For the optimal AA′ stacking mode at the equilibrium interlayer distance of 3.33 Å, the lattice summed electrostatic potential becomes extremely small (left panel). Due to symmetry considerations, the electrostatic potential above the center of the hexagon and above the center of a B−N bond vanishes identically (right panel).

approximately proportional to the circumference of a ring of radius r and thus increases linearly with the r. Thus, as previously discussed,[5,6,59−69] in order to map the classical electrostatic potential above an infinite *h*-BN layer resulting from the atom-centered electronic monopole contributions and the nuclear charges, it is necessary to perform a full lattice sum over all partially charged lattice sites within the sheet. This sum is given by the following general expression:

$$\varphi(\vec{r}) = \sum_{i=1}^{d} \sum_{n=-\infty}^{\infty} \sum_{m=-\infty}^{\infty} (q_i/[(x - x_i - nT_1^x - mT_2^x)^2 + (y - y_i - nT_1^y - mT_2^y)^2 + (z - z_i)^2]^{1/2}) \quad (1)$$

where, $\varphi(\vec{r})$ is the electrostatic potential, in atomic units, at point $\vec{r} = (x,y,z)$ in space due to $q_{i=1,...,d}$ charges located at points $\vec{r}_i = (x_i,y_i,z_i)$ within the two-dimensional periodic unit cell with lattice vectors $\vec{T}_1 = (T_1^x,T_1^y)$ and $\vec{T}_2 = (T_2^x,T_2^y)$. We note that $\varphi(\vec{r})$ diverges when measured at the lattice sites. For simplicity, we choose a rectangular unit cell (see right panel of Figure 2) with lattice vectors $\vec{T}_1 = (\sqrt{3},0)a$ and $\vec{T}_2 = (0,3)a$, a = 1.446 Å being the B−N bond length, atomic positions $\vec{r}_1 = (0,0,0)$, $\vec{r}_2 = (0,1,0)a$, $\vec{r}_3 = (1/2)(\sqrt{3},3,0)a$, and $\vec{r}_4 = (1/2)(\sqrt{3},5,0)a$, and charges $q_1 = -q_2 = q_3 = -q_4 = \delta$ where $\delta = -0.5$.[8,59] Unfortunately, for charge neutral unit cells ($\sum_{i=1}^{d} q_i = 0$), the sum appearing in eq 1 is conditionally convergent and therefore challenging to evaluate using direct summation. An elegant way to circumvent this problem was proposed by Ewald where the conditionally convergent lattice sum is converted into two absolutely converging sums, one in real space and the other in reciprocal space.[70,71] Using this technique (see Supporting Information for a detailed derivation), one is able to efficiently calculate the electrostatic potential due to all partially charged atomic centers at any point above the two-dimensional infinite *h*-BN lattice.

To study this electrostatic contribution at the optimal AA′ stacking mode, the potential above a nitrogen atomic site is plotted as a function of the distance from the *h*-BN layer. In the left panel of Figure 2, the full lattice-sum results are compared to the electrostatic potential produced by an isolated partially charged nitrogen atomic center. Clearly, the collective electrostatic potential decays exponentially (see Supporting Information) and much faster than $-\delta/r$, becoming extremely small at the equilibrium interlayer distance in agreement with similar results obtained by Green et al.[6] At shorter distances, Pauli repulsions become dominant and prevent the layers from approaching each other, thus rendering the region, where partial atomic charges contributions become substantial for binding, physically irrelevant. At the optimal AA′ stacking mode with the interlayer distance set to 3.33 Å, the calculated electrostatic potential energy due to the partially charged atomic centers is 8.4×10^{-4} eV/atom, which is merely a negligible fraction of the total bilayer binding energy in the presence of vdW interactions calculated to be 26.0−38.1 meV/atom.[8,24] A full map of this electrostatic potential 3.33 Å above the *h*-BN surface is presented in the right panel of Figure 2. Due to symmetry considerations, the potential vanishes identically above the centers of the hexagons and above the centers of the B−N bonds regardless of the distance from the surface. At other positions along the surface, the potential is nonzero and preserves the hexagonal lattice symmetry with values not exceeding 8.4×10^{-4} eV/atom.

III. FULL NON-DISPERSIVE INTERLAYER INTERACTION ANALYSIS

On the basis of the above considerations, it is now clear that due to the long-range nature of the Coulomb potential, the overall classical electrostatic interactions between partially charged atomic centers have only a marginal effect on the interlayer binding in *h*-BN. One may therefore conclude that the main classical electrostatic contribution to the interlayer binding in both graphene and *h*-BN comes from higher order multipole interactions.[5] Since the intralayer hexagonal lattice structures of the two materials are nearly identical, it is tempting to assume that these contributions would be very similar. This, however, is not trivial, as both the optimal stacking mode and the overall density profile in the two materials are quite different.[54,56] Furthermore, other nonclassical contributions such as Pauli repulsions which prevent the layers from sticking together[16] and the exchange-correlation terms appearing in

density functional theory (DFT) calculations can considerably differ between the two materials. Thus, in order to gain a better understanding of the separate roles of the different contributions to the interlayer binding, DFT-based binding energy calculations for bilayer graphene and *h*-BN have been performed. In order to avoid ambiguities in the definition of the different components of the total energy resulting from the lattice sums performed in periodic boundary conditions calculations, a set of finite-sized bilayer clusters with hexagonal symmetry and increasing diameter has been chosen. For the *h*-BN system, zigzag edged hydrogen terminated hexagonal clusters have been considered (see right panel of Figure 3); test calculations with

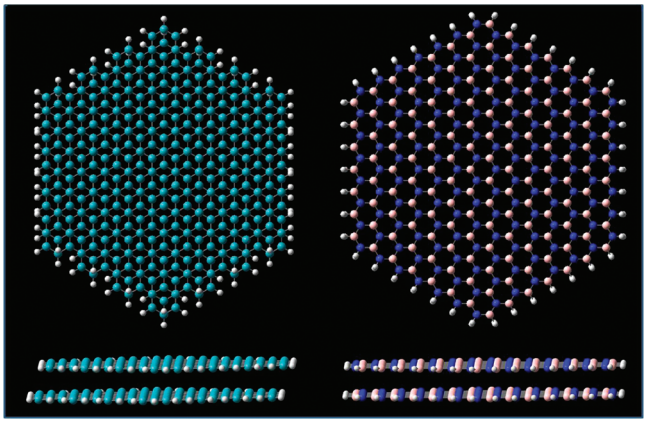

Figure 3. Top (upper panels) and side (lower panels) views of the largest bilayer graphene armchair flakes (left) and bilayer *h*-BN zigzag flakes (right) used in the present study. The graphene system consists of a total of 528 atoms, and the *h*-BN system has a total of 672 atoms. Cyan, blue, pink, and gray spheres represent carbon, boron, nitrogen, and hydrogen atoms, respectively.

armchair *h*-BN clusters revealed similar results to those obtained with the zigzag clusters (see Supporting Information). In order to prevent the occurrence of edge states in the bilayer graphene system,[12,72−76] hydrogen terminated armchair graphene dimers have been considered (see left panel of Figure 3). Each hexagonal cluster was cut out of the relevant pristine periodic layer with C−C and B−N bond lengths of 1.420 Å and 1.446 Å, respectively. The bare edges were hydrogen terminated with benzene C−H and borazine B−H and N−H bond lengths of 1.101 Å, 1.200 Å, and 1.020 Å, respectively. The individual flakes were then appropriately combined to form a finite sized AB stacked graphene dimer and AA′ stacked *h*-BN dimer. No geometry optimization was performed. The cluster size was increased until edge effects on the calculated binding energies became marginal (see Supporting Information). All calculations were carried out using the Gaussian 09 suite of programs[77] with the double-ζ polarized 6-31G** Gaussian basis set[78] utilizing the counter-poise correction[79,80] to eliminate possible basis set superposition errors. Tests for convergence of the results with respect to the basis sets were performed for the smaller flakes, indicating convergence of the total binding energy down to ∼1 meV/atom at physically relevant interlayer separations (see Supporting Information).

Figure 4 presents the dependence of the different components of the total DFT energy on the interlayer distance in graphene and *h*-BN. Here, E_{El} is the sum of classical electrostatic contributions (nuclear−nuclear repulsion, electron−nuclear attraction, and the Hartree term), E_{xc} is the sum of exchange and correlation DFT contributions, E_k is the kinetic energy term, and E_T is the total energy. Three exchange-correlation density functional approximations are considered:[81] (i) the generalized gradient corrected PBE functional[82] representing semilocal functionals, (ii) the hybrid B3LYP functional[83] aimed at partly eliminating the self-interaction error appearing in semilocal functionals and regaining some of the correct long-range exchange behavior, which is relevant for the present study, and (iii) the semiempirical hybrid meta-GGA M06 functional[84,85] parametrized to mimic some of the nonlocal correlation required to describe dispersion interactions. All functional approximations considered lack the proper treatment of long-range correlation effects responsible for dispersive vdW interactions and are therefore limited to a description of classical electrostatic, exchange, short (or middle)-range (SR) correlation, and Pauli repulsions effects on the interlayer binding.[86]

As can be seen, all three functional approximations predict that the E_{El} contributions (red squares) are much larger than the classical electrostatic energy due to the partially charged atomic centers in *h*-BN (brown x marks) at physically relevant interlayer distances of the two materials. Nevertheless, PBE and B3LYP predict that the combined electrostatic, exchange, and SR-correlation (green diamonds) contributions to the total binding energy at these distances are almost completely canceled out by the kinetic energy term (blue triangles) partly manifesting the effects of Pauli repulsions.[16] As a result, the total binding energy curves (black circles) calculated by both functionals, which, as described above, lack the dispersive component, are completely nonbonding for graphene and very weakly bonding for *h*-BN. This is consistent with recently reported results for graphite[87] and molecular graphene derivatives adsorbed on graphene.[16] As may be expected, the binding energy curve of the M06 functional, which by construction incorporates some middle-range correlation, is binding throughout the interlayer distance regime considered for the two materials.[86]

The PBE calculations suggest that the dependence of the exchange-SR-correlation contributions on the interlayer distance in both materials is very similar, whereas the electrostatic and kinetic energy terms of graphene and *h*-BN behave quite differently. This implies that the similarity of the total (vdW lacking) binding energy curves of the two materials results from a coincidental cancellation of the different terms. The B3LYP results reveal a completely different picture where the interlayer distance dependences of all calculated energy components in both materials are very similar (with minor deviations between the kinetic energy terms). This suggests that the similarity between the total nondispersive interlayer binding curves originates from the physical similarity of the two materials and not from a fortuitous cancellation of the different terms. Notably, the overall differences between the total binding energies calculated using the two nondispersive functional approximations at the equilibrium interlayer distance are merely 5 meV/atom, which is close to the accuracy limit that can be expected from such calculations.

The interlayer distance dependence of the M06 energy components considerably differs from that obtained by the other two functional approximations. Nevertheless, similar to the B3LYP results, the two materials exhibit very similar electrostatic behavior throughout the entire interlayer distances regime studied apart from some deviations at very short distances. Interestingly, despite the differences in the M06 exchange-correlation and kinetic energy terms of the two materials, the overall difference between the two M06 binding energy curves is ∼5 meV/atom at the equilibrium interlayer distance. These

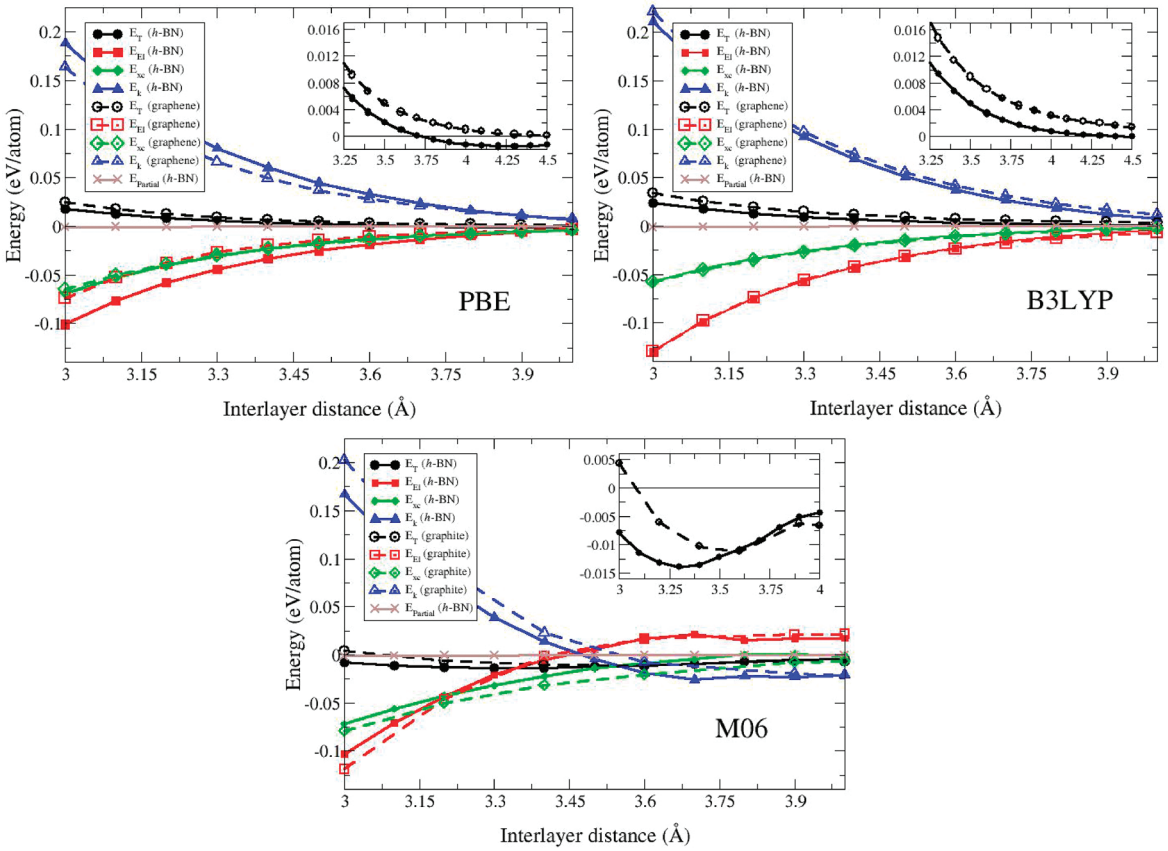

Figure 4. Dependence of the total (black circles), electrostatic (red squares), exchange-SR-correlation (green diamonds), and kinetic (blue triangles) DFT energy components on the interlayer distance of bilayer *h*-BN (solid lines, full symbols) and bilayer graphene (dashed lines, open symbols) calculated using the PBE (upper left panel), B3LYP (upper right panel), and M06 (lower panel) density functional approximations. The electrostatic energy due to interlayer interactions between partially charged atomic centers is presented for comparison (brown x marks). Zero energy is defined as the value of the relevant component at infinite separation. Insets: zoom on the interlayer dependence of the calculated total energies. PBE results for bilayer graphene (*h*-BN) were obtained using the 528 (672) atom cluster presented in the left (right) panel of Figure 3. B3LYP and M06 results for bilayer graphene and *h*-BN were obtained using 528 and 240 atom clusters, respectively (see Supporting Information).

findings along with the results of the nondispersive functionals suggest that the similarity in the interlayer interactions of graphene and *h*-BN results from a simultaneous similarity between their nondispersive and dispersive interaction terms.

It should be noted that in principle DFT should give the true electron density, and thus the Hartree and electron−nuclear terms appearing in E_{El} should provide accurate measures of the classical interlayer electron−electron and electron−nuclear energies.[88] However, when using approximate exchange-correlation density functionals, care should be taken when ascribing a direct physical interpretation to the calculated electrostatic (and kinetic) Kohn−Sham energy trems.[89] This is clearly evident from the differences in the calculated electrostatic energies obtained using the PBE, B3LYP, and M06 functionals in Figure 4. These differences arise from variations in the intralayer electron density profile obtained by the various functional approximations and the different long-range behaviors, resulting in a functional dependent self-consistent balance between the obtained interlayer electrostatic, exchange-correlation, and kinetic energies. Nevertheless, the notable similarity between all B3LYP binding energy components and the M06 electrostatic energies of the two materials does provide an indication that higher order classical electrostatic multipole interlayer interactions in the two materials should be similar as well. Furthermore, the mutual cancellation of the different energy components of both nondispersive functional approximations at the equilibrium interlayer distance suggests that vdW interactions are responsible for anchoring the layers in both materials.[1,8,16]

IV. VAN DER WAALS INTERACTIONS

The analysis presented above establishes the fact that electrostatic interactions between the partially charged atomic cores in *h*-BN, which are absent in graphene, have a minor contribution to the interlayer binding due to the rapid decay of the potential into the vacuum above the layer. Furthermore, it shows that at physically relevant interlayer distances in graphene and *h*-BN, the overall classical electrostatic and exchange-SR-correlation DFT contributions (which by themselves can be quite significant) almost completely cancel out with the kinetic energy term, partly manifesting the effect of Pauli repulsions. This suggests, as we previously concluded, that vdW interactions are a crucial ingredient for anchoring the graphene and *h*-BN layers at their equilibrium interlayer distance.[1,8] Since the experimental interlayer distances in both systems are essentially the same, one may deduce that the attractive vdW interactions in both systems are similar. As mentioned above, this conclusion is somewhat surprising in light of the different static polarizabilities presented by the carbon, boron, and nitrogen atoms.

In order to gain quantitative understanding regarding the role of vdW interactions for the interlayer binding in the two materials, the C_6/R^6 leading dispersion term should be considered. To this end, the Tkatchenko−Scheffler vdW

(TS-vdW) correction scheme to density functional theory may be used.[90,91] Here, the pairwise bulk C_6 coefficients between atoms A and B are calculated using the following relation:[90]

$$C_{6,AB} = \frac{2C_{6,A}C_{6,B}}{\frac{\alpha_B}{\alpha_A}C_{6,A} + \frac{\alpha_A}{\alpha_B}C_{6,B}} \quad (2)$$

where α_i is the bulk static polarizability and $C_{6,i}$ is the homonuclear pairwise bulk coefficient of atom i = A and B. The homonuclear bulk polarizabilities and coefficients can be obtained from the free atom values (α_i^0 and $C_{6,i}^0$, respectively) via

$$\alpha_i = \left(\frac{V_i^{\text{eff}}}{V_i^{\text{free}}}\right)\alpha_i^0;\ C_{6,i} = \left(\frac{V_i^{\text{eff}}}{V_i^{\text{free}}}\right)^2 C_{6,i}^0 \quad (3)$$

where V_i^{eff} is the effective volume of atom i in the bulk system referenced to the free atom volume in vacuo, V_i^{free}. The relative effective volume, in turn, is estimated using the Hirshfeld partitioning scheme applied to the electron density obtained from a density functional theory calculation.[92]

The free-atom parameters may be obtained from the database presented by Chu and Dalgarno,[93] constructed using self-interaction corrected time dependent density functional theory calculations. Values for the relevant atoms are summarized in the Table 1.

Table 1. Values for the Free Atom Dipole Polarizabilities, C_6 Coefficients, and Relative Effective Hirshfeld Volumes of Carbon, Boron, and Nitrogen Atoms Relevant for the Present Study

	C	B	N
α^0 (a.u.)[93]	12.0	21.0	7.4
C_6^0 (a.u.)[93]	46.6	99.5	24.2
$V_i^{\text{eff}}/V_i^{\text{free}}$[94]	0.850 (graphite)	0.811 (*h*-BN)	0.879 (*h*-BN)

Table 2 summarizes the numerical values for the pairwise bulk (graphite and *h*-BN) C_6 coefficients obtained using eqs 2 and 3 with the parameters presented in Table 1. At the optimal AA′ stacking mode of *h*-BN and the AB mode of graphite, the most prominent C_6 contributions come from the eclipsed boron−nitrogen (in *h*-BN) and carbon−carbon (in graphite) atomic centers attraction on adjacent layers. As can be seen, despite the large differences between the C−C, B−B, and N−N coefficients, the C−C and B−N coefficient agree to within less than 2%, indicating that indeed the vdW interactions in graphite and *h*-BN should be very similar in nature.

Table 2. Values (in Hartree·Bohr^6) for the Pair-Wise Bulk C_6 Coefficients Obtained Using eqs 2 and 3 and the Parameters of Table 1 for Carbon, Boron, and Nitrogen Atoms[a]

B−B	N−N	C−C	B−N	C−B	C−N
65.4	**18.7**	**33.7**	**33.1**	46.2	24.8

[a]Values relevant for the present study are presented in bold.

To further investigate the vdW contribution beyond the eclipsed atom interactions, an analysis of the full vdW interaction scheme of the bilayer systems is presented in Figure 5 where the *h*-BN bilayer is assumed to be at the AA′ stacking mode and the bilayer graphene at the AB mode. Different components of the vdW energy are considered separately. The term "mixed sublattice" interactions in *h*-BN refers to the vdW energy contribution of a single boron (nitrogen) atom in one *h*-BN layer with all nitrogen (boron) atoms in the other layer (marked as BN). In bilayer graphene, this term refers to the interaction of a single carbon atom located at a given sublattice site of one graphene layer with all carbon atoms belonging to the other sublattice sites of the second graphene layer (marked as CC′ or C′C). Respectively, the term "same sublattice" interactions in *h*-BN refers to the vdW contribution of a single boron (nitrogen) atom in one *h*-BN layer with all boron (nitrogen) atoms in the other layer (marked as BB or NN). In bilayer graphene, this term refers to the interaction of a single carbon atom located in a given sublattice site of one graphene layer with all carbon atoms belonging to the same sublattice sites of the second graphene layer (marked as CC or C′C′).

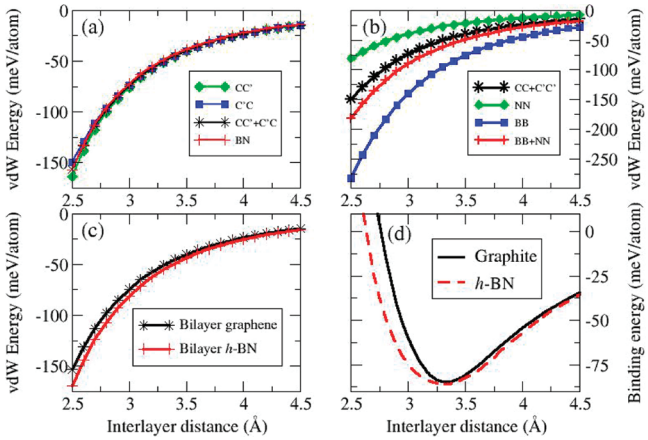

Figure 5. vdW contributions to the binding energy curves of graphite and *h*-BN in the AB and AA′ stacking modes, respectively. (a) Mixed sublattice contributions to the vdW energy of the bilayer systems. CC′ represents the interaction of a single carbon atom located on sublattice 1 of the first layer with all carbon atoms located on sublattice 2 of the second layer. C′C represents the interaction of a single carbon atom located on sublattice 2 of the first layer with all carbon atoms located on sublattice 1 of the second layer. CC′+C′C represents the overall sum of the CC′ and C′C contribution per atom. BN stands for the interaction of a single boron (nitrogen) atom in one *h*-BN layer with all nitrogen (boron) atoms in the other layer. (b) Same sublattice contributions to the vdW energy of the bilayer systems. CC+C′C′ represent the overall sum of the interaction of a single carbon atom located on sublattice 1 of the first layer with all carbon atoms located on the same sublattice of the second layer and the interaction of a single carbon atom located on sublattice 2 of the first layer with all carbon atoms located on sublattice 2 of the second layer. Due to the symmetry of the hexagonal lattice, the CC and C′C′ contributions are identical to each other and therefore also to the CC+C′C′ contribution per atom. NN (BB) represents the interaction of a single boron (nitrogen) atom in one layer with all boron (nitrogen) atoms in the second layer. BB+NN represents the sum of the BB and NN vdW contributions per atom. (c) Total vdW energy per atom of the bilayer systems. See Supporting Information for further details regarding this calculation. (d) Full binding energy curves of bulk graphite[1] (solid black line) and bulk *h*-BN[8] (red dashed line) as calculated using the TS-vdW method. Results for the graphite binding energy calculations have been provided courtesy of Felix Hanke.

Panel a of Figure 5 shows the vdW energy contribution of the mixed sublattice interactions of a single atom in one layer with all relevant atoms in the other layer of the bilayer systems. While graphite and *h*-BN present different optimal stacking modes, the vdW energy only weakly depends on the exact stacking of the hexagonal lattices.[17] Therefore, since the C−C

dx.doi.org/10.1021/ct200880m | J. Chem. Theory Comput. 2012, 8, 1360−1369

and B−N C_6 coefficients were found to be very similar, the vdW contributions of the mixed interactions of both systems are nearly identical. Similarly, panel b of Figure 5 shows the vdW energy contribution of the same sublattice interactions. Here, due to the large differences between the C−C, B−B, and N−N C_6 coefficients, the separate contribution of each of the sublattice interactions is quite different. Nevertheless, when adding the contributions of the BB and NN interactions in *h*-BN and the CC and C′C′ interactions in bilayer graphene, the overall contributions are very similar, reflecting the fact that the C−C C_6 coefficient is close to the average value of the B−B and N−N coefficients. Thus, as shown in panel c of Figure 3, owing to the isoelectronic nature of the two materials, their similar intralayer bond lengths and lattice structures, and the ordering of the atomic static polarizabilities, the overall vdW attraction per atom in the unit cell of bilayer graphene and *h*-BN are very similar despite the differences in the individual C_6 coefficients of the different atoms.

Finally, these results are clearly manifested in the full binding energy curves presented in panel d of Figure 5 for bulk graphite (calculated by Hanke[1]) and *h*-BN (calculated by Marom et al.[8]) as obtained using the TS-vdW scheme. As can be seen, both binding energy curves predict the same interlayer distance of 3.33 Å, in excellent agreement with the experimental values[45−53] and similar binding energies (graphite, 84.7 meV/atom; *h*-BN, 85.9 meV/atom). The dispersive attractive part of both systems is very similar, whereas the main deviations between the two curves appear in the short range where Pauli repulsions due to overlap of the B−N electron clouds in *h*-BN and C−C electron clouds in graphite become dominant. These deviations are to be expected, as the two materials possess different optimal stacking modes and since the effective volumes of carbon in graphite and boron and nitrogen in *h*-BN are different.

V. SUMMARY AND CONCLUSIONS

To summarize, in the present study, the interlayer binding in graphene and *h*-BN was compared. It was found that despite the polar nature of the B−N bond in *h*-BN, the full lattice sum of the electrostatic contributions from the effective charges on all atomic sites within the layer results in rapid exponential decay of the electrostatic potential into the vacuum. As a result, at the equilibrium interlayer distance, the overall classical electrostatic contribution from the interaction between all partially charged atomic centers to the interlayer binding is merely a small fraction of the total calculated binding energy. At physically relevant interlayer distances, the contribution of electrostatic and exchange-SR-correlation DFT energy terms elegantly cancels out the kinetic energy term partly manifesting the effect of Pauli repulsions. Nonetheless, when considering relative lateral shifts of the layers at the equilibrium interlayer distance, the residual electrostatic potential along with the Pauli repulsions are sufficient to set the AA′ stacking mode as the optimal configuration of *h*-BN. The opposite holds true for the dispersive component, which has a minor effect on the corrugation of the interlayer sliding energy surface[8,17] but is a crucial factor for the interlayer anchoring in both systems.[8,16] Here, despite notable differences between the free-atom as well as the bulk homonuclear C_6 coefficients of the two materials, the heteroatomic bulk coefficients in *h*-BN agree to within 2% with the C−C coefficients in bulk graphite. This translates to very similar binding energy curves for both materials (deviating mainly at distances shorter than the equilibrium interlayer distance where Pauli repulsions become dominant), thus resulting in similar binding energies and practically identical equilibrium interlayer distances for graphene and *h*-BN. These conclusions are further supported by recent studies of *h*-BN/graphene hybrid structures,[95−101] which, similar to graphite and *h*-BN, should present an interlayer distance of ∼3.3 Å.[96]

Some notes regarding the calculations presented in this study should be made: (i) When performing the electrostatic (and vdW) sums only the pristine systems have been considered. Defects, such as lattice vacancies,[33,102] may introduce long-range effective Coulomb potentials which decay asymptotically as α/r rather than exponentially into the vacuum. (ii) The bulk TS-vdW calculations presented above lack a proper description of the screening of the pairwise interaction by the dielectric medium and nonadditive many-body vdW energy contributions. The neglect of screening effects usually results in too large bulk C_6 coefficients and therefore overestimates binding energy values, but it often still produces accurate structural properties for molecular dimers, molecular crystals, and layered materials.[1,8,15,16,23,24,86,90,91,103−107] As screening effects on the unscreened C_6 coefficients are expected to be similar in graphite and *h*-BN, which have the same intralayer hexagonal lattice structure, the inclusion of such effects is expected to influence the binding energy curves of both materials in a similar manner, thus leaving the conclusions drawn here, based on the unscreened coefficients, valid. (iii) The TS-vdW approach, which relies on additive pairwise contributions, does not capture the correct asymptotic form of vdW interactions between graphene layers.[15] However, the present study focuses on the region near the interlayer equilibrium separation where, as mentioned above, the ability of this approach to accurately treat dispersive interactions is well established. We note that the proper description of the above-mentioned effects is a subject of ongoing research.

Finally, a note should be made regarding the general nature of the conclusions drawn above. The rapid decay of the electrostatic potential due to the partially charged atomic centers into the vacuum above the two-dimensional layer is not a unique property of the hexagonal lattice of *h*-BN.[61] While its fine details are expected to depend on the chemical composition and structural topology of the underlying material, the general nature of the exponential decay is expected to prevail in many layered systems (see Supporting Information). In contrast, the contribution of higher-order classical electrostatic multipole interactions, exchange-SR-correlation energies, Pauli repulsions, and vdW attraction at different interlayer distances may heavily depend on the specific chemical nature of the material and its lattice structure. Therefore, when studying the interlayer binding in such materials, a careful balance between electrostatic, dispersive, and Pauli interactions should be considered.

■ ASSOCIATED CONTENT

Supporting Information

(i) Convergence tests for the cluster DFT calculations, (ii) a detailed derivation of the Ewald summation method for the electrostatic potential of an infinite (quasi-)two-dimensional sheet of point charges, (iii) implementation of the Ewald summation method for the electrostatic potential above an infinite two-dimensional *h*-BN layer due to the partially charged atomic centers, (iv) derivation of a formula for the calculation of the total Coulomb binding energy of an infinite *h*-BN bilayer due to interlayer interaction between partially charged atomic centers, and (v) derivation of a formula for the calculation of the total vdW binding energy of infinite bilayer graphene and

h-BN. This information is available free of charge via the Internet at http://pubs.acs.org

AUTHOR INFORMATION

Corresponding Author

*E-mail: odedhod@tau.ac.il.

Notes

The authors declare no competing financial interest.

ACKNOWLEDGMENTS

The author would like to thank Dr. Alexandre Tkatchenko and Dr. Felix Hanke for generously sharing results of their calculations and for many valuable discussions. Many thanks to Prof. Ernesto Joselevich, Prof. Leeor Kronik, Prof. Haim Diamant, Prof. Shahar Hod, Prof. Fernando Patolsky, Dr. Noa Marom, Mr. Guy Cohen, and Mr. Tal Levy for fruitful discussions regarding the subject. This work was supported by the Israel Science Foundation under grant no. 1313/08, the Center for Nanoscience and Nanotechnology at Tel Aviv University, and the Lise Meitner-Minerva Center for Computational Quantum Chemistry. The research leading to these results has received funding from the European Community's Seventh Framework Programme FP7/2007-2013 under grant agreement no. 249225.

REFERENCES

(1) Hanke, F. Sensitivity Analysis and Uncertainty Calculation for Dispersion Corrected Density Functional Theory. *J. Comput. Chem.* **2011**, *32*, 1424−1430.

(2) Onodera, T.; Morita, Y.; Nagumo, R.; Miura, R.; Suzuki, A.; Tsuboi, H.; Hatakeyama, N.; Endou, A.; Takaba, H.; Dassenoy, F.; Minfray, C.; Joly-Pottuz, L.; Kubo, M.; Martin, J.-M.; Miyamoto, A. A Computational Chemistry Study on Friction of h-MoS2. Part II. Friction Anisotropy. *J. Phys. Chem. B* **2010**, *114*, 15832−15838.

(3) Onodera, T.; Morita, Y.; Suzuki, A.; Koyama, M.; Tsuboi, H.; Hatakeyama, N.; Endou, A.; Takaba, H.; Kubo, M.; Dassenoy, F.; Minfray, C.; Joly-Pottuz, L.; Martin, J.-M.; Miyamoto, A. A Computational Chemistry Study on Friction of h-MoS2. Part I. Mechanism of Single Sheet Lubrication. *J. Phys. Chem. B* **2009**, *113*, 16526−16536.

(4) Ghosh, P. N.; Maiti, C. R. Interlayer Potential in 2H-MoS2. *Phys. Rev. B* **1984**, *29*, 4757.

(5) Kuzuba, T.; Sato, T.; Ishii, T.; Arai, T. Interlayer Binding of Hexagonal Boron Nitride in the Rigid-Layer Approximation. *Phys. Rev. B* **1985**, *32*, 1230.

(6) Green, J. F.; Bolland, T. K.; Bolland, J. W. Theoretical Elastic Behavior for Hexagonal Boron Nitride. *J. Chem. Phys.* **1976**, *64*, 656−662.

(7) Hod, O. Quantifying the Stacking Registry Matching in Layered Materials. *Isr. J. Chem.* **2010**, *50*, 506−514.

(8) Marom, N.; Bernstein, J.; Garel, J.; Tkatchenko, A.; Joselevich, E.; Kronik, L.; Hod, O. Stacking and Registry Effects in Layered Materials: The Case of Hexagonal Boron Nitride. *Phys. Rev. Lett.* **2010**, *105*, 046801.

(9) Novoselov, K. S.; Geim, A. K.; Morozov, S. V.; Jiang, D.; Zhang, Y.; Dubonos, S. V.; Grigorieva, I. V.; Firsov, A. A. Electric Field Effect in Atomically Thin Carbon Films. *Science* **2004**, *306*, 666−669.

(10) Geim, A. K.; Novoselov, K. S. The Rise of Graphene. *Nat. Mater.* **2007**, *6*, 183−191.

(11) Castro Neto, A. H.; Guinea, F.; Peres, N. M. R.; Novoselov, K. S.; Geim, A. K. The Electronic Properties of Graphene. *Rev. Mod. Phys.* **2009**, *81*, 109.

(12) Barone, V.; Hod, O.; Peralta, J. E.; Scuseria, G. E. Accurate Prediction of the Electronic Properties of Low-Dimensional Graphene Derivatives Using a Screened Hybrid Density Functional. *Acc. Chem. Res.* **2011**, *44*, 269−279.

(13) Iijima, S. Helical Microtubules of Graphitic Carbon. *Nature* **1991**, *354*, 56−58.

(14) Charlier, J.-C.; Gonze, X.; Michenaud, J.-P. Graphite Interplanar Bonding: Electronic Delocalization and van der Waals Interaction. *Europhys. Lett.* **1994**, *28*, 403.

(15) Lebegue, S.; Harl, J.; Gould, T.; Angyan, J. G.; Kresse, G.; Dobson, J. F. Cohesive Properties and Asymptotics of the Dispersion Interaction in Graphite by the Random Phase Approximation. *Phys. Rev. Lett.* **2010**, *105*, 196401.

(16) Björk, J.; Hanke, F.; Palma, C.-A.; Samori, P.; Cecchini, M.; Persson, M. Adsorption of Aromatic and Anti-Aromatic Systems on Graphene through $\pi-\pi$ Stacking. *J. Phys. Chem. Lett.* **2010**, *1*, 3407−3412.

(17) Kolmogorov, A. N.; Crespi, V. H. Registry-Dependent Interlayer Potential for Graphitic Systems. *Phys. Rev. B* **2005**, *71*, 235415.

(18) Hasegawa, M.; Nishidate, K. Semiempirical Approach to the Energetics of Interlayer Binding in Graphite. *Phys. Rev. B* **2004**, *70*, 205431.

(19) Palser, A. H. R. Interlayer Interactions in Graphite and Carbon Nanotubes. *Phys. Chem. Chem. Phys.* **1999**, *1*, 4459−4464.

(20) Carlson, A.; Dumitrică, T. Extended Tight-Binding Potential for Modelling Intertube Interactions in Carbon Nanotubes. *Nanotechnology* **2007**, *18*, 065706.

(21) Cumings, J.; Zettl, A. Low-Friction Nanoscale Linear Bearing Realized from Multiwall Carbon Nanotubes. *Science* **2000**, *289*, 602−604.

(22) Buldum, A.; Lu, J. P. Atomic Scale Sliding and Rolling of Carbon Nanotubes. *Phys. Rev. Lett.* **1999**, *83*, 5050.

(23) Spanu, L.; Sorella, S.; Galli, G. Nature and Strength of Interlayer Binding in Graphite. *Phys. Rev. Lett.* **2009**, *103*, 196401.

(24) Rydberg, H.; Dion, M.; Jacobson, N.; Schroder, E.; Hyldgaard, P.; Simak, S. I.; Langreth, D. C.; Lundqvist, B. I. Van der Waals Density Functional for Layered Structures. *Phys. Rev. Lett.* **2003**, *91*, 126402.

(25) Ortmann, F.; Bechstedt, F.; Schmidt, W. G. Semiempirical van der Waals Correction to the Density Functional Description of Solids and Molecular Structures. *Phys. Rev. B* **2006**, *73*, 205101.

(26) Rydberg, H.; Jacobson, N.; Hyldgaard, P.; Simak, S. I.; Lundqvist, B. I.; Langreth, D. C. Hard Numbers on Soft Matter. *Surf. Sci.* **2003**, *532*−*535*, 606−610.

(27) Zeng, H.; Zhi, C.; Zhang, Z.; Wei, X.; Wang, X.; Guo, W.; Bando, Y.; Golberg, D. White Graphenes": Boron Nitride Nanoribbons via Boron Nitride Nanotube Unwrapping. *Nano Lett.* **2010**, *10*, 5049−5055.

(28) Song, L.; Ci, L.; Lu, H.; Sorokin, P. B.; Jin, C.; Ni, J.; Kvashnin, A. G.; Kvashnin, D. G.; Lou, J.; Yakobson, B. I.; Ajayan, P. M. Large Scale Growth and Characterization of Atomic Hexagonal Boron Nitride Layers. *Nano Lett.* **2010**, *10*, 3209−3215.

(29) Ooi, N.; Rairkar, A.; Lindsley, L.; Adams, J. B. Electronic Structure and Bonding in Hexagonal Boron Nitride. *J. Phys.: Condens. Matter* **2006**, *18*, 97.

(30) Alem, N.; Erni, R.; Kisielowski, C.; Rossell, M. D.; Gannett, W.; Zettl, A. Atomically Thin Hexagonal Boron Nitride Probed by Ultrahigh-Resolution Transmission Electron Microscopy. *Phys. Rev. B* **2009**, *80*, 155425.

(31) Pacile, D.; Meyer, J. C.; Girit, C. O.; Zettl, A. The Two-Dimensional Phase of Boron Nitride: Few-Atomic-Layer Sheets and Suspended Membranes. *Appl. Phys. Lett.* **2008**, *92*, 133107−3.

(32) Han, W.-Q.; Wu, L.; Zhu, Y.; Watanabe, K.; Taniguchi, T. Structure of Chemically Derived Mono- and Few-Atomic-Layer Boron Nitride Sheets. *Appl. Phys. Lett.* **2008**, *93*, 223103−3.

(33) Meyer, J. C.; Chuvilin, A.; Algara-Siller, G.; Biskupek, J.; Kaiser, U. Selective Sputtering and Atomic Resolution Imaging of Atomically Thin Boron Nitride Membranes. *Nano Lett.* **2009**, *9*, 2683−2689.

(34) Zhi, C.; Bando, Y.; Tang, C.; Kuwahara, H.; Golberg, D. Large-Scale Fabrication of Boron Nitride Nanosheets and Their Utilization in Polymeric Composites with Improved Thermal and Mechanical Properties. *Adv. Mater.* **2009**, *21*, 2889−2893.

(35) Novoselov, K. S.; Jiang, D.; Schedin, F.; Booth, T. J.; Khotkevich, V. V.; Morozov, S. V.; Geim, A. K. Two-Dimensional Atomic Crystals. *Proc. Natl. Acad. Sci. U.S.A.* **2005**, *102*, 10451−10453.
(36) Jin, C.; Lin, F.; Suenaga, K.; Iijima, S. Fabrication of a Freestanding Boron Nitride Single Layer and Its Defect Assignments. *Phys. Rev. Lett.* **2009**, *102*, 195505.
(37) Lee, C.; Li, Q.; Kalb, W.; Liu, X.-Z.; Berger, H.; Carpick, R. W.; Hone, J. Frictional Characteristics of Atomically Thin Sheets. *Science* **2010**, *328*, 76−80.
(38) Gorbachev, R. V.; Riaz, I.; Nair, R. R.; Jalil, R.; Britnell, L.; Belle, B. D.; Hill, E. W.; Novoselov, K. S.; Watanabe, K.; Taniguchi, T.; Geim, A. K.; Blake, P. Hunting for Monolayer Boron Nitride: Optical and Raman Signatures. *Small* **2011**, *7*, 465−468.
(39) Ribeiro, R. M.; Peres, N. M. R. Stability of Boron Nitride Bilayers: Ground-State Energies, Interlayer Distances, and Tight-Binding Description. *Phys. Rev. B* **2011**, *83*, 235312.
(40) Warner, J. H.; Rümmeli, M. H.; Bachmatiuk, A.; Büchner, B. Atomic Resolution Imaging and Topography of Boron Nitride Sheets Produced by Chemical Exfoliation. *ACS Nano* **2010**, *4*, 1299−1304.
(41) Qi, Y.; Hector, J. L. G. Planar Stacking Effect on Elastic Stability of Hexagonal Boron Nitride. *Appl. Phys. Lett.* **2007**, *90*, 081922−3.
(42) Topsakal, M.; Akturk, E.; Ciraci, S. First-Principles Study of Two- and One-Dimensional Honeycomb Structures of Boron Nitride. *Phys. Rev. B* **2009**, *79*, 115442.
(43) Taylor, R.; Coulson, C. A. Studies in Graphite and Related Compounds III: Electronic Band Structure in Boron Nitride. *Proc. Phys. Soc., Ser. A* **1952**, *65*, 834.
(44) Lopatin, V. V.; Shcherbina, V. P. Nature of the Interlayer Interaction in Hexagonal Boron Nitride. *J. Struct. Chem.* **1988**, *29*, 466−469.
(45) Bernal, J. D. The Structure of Graphite. *Proc. R. Soc. London, Ser. A* **1924**, *106*, 749−773.
(46) Chung, D. Review Graphite. *J. Mater. Sci.* **2002**, *37*, 1475−1489.
(47) Baskin, Y.; Meyer, L. Lattice Constants of Graphite at Low Temperatures. *Phys. Rev.* **1955**, *100*, 544.
(48) Solozhenko, V. L.; Will, G.; Elf, F. Isothermal Compression of Hexagonal Graphite-Like Boron Nitride up to 12 GPa. *Solid State Commun.* **1995**, *96*, 1−3.
(49) Paszkowicz, W.; Pelka, J. B.; Knapp, M.; Szyszko, T.; Podsiadlo, S. Lattice Parameters and Anisotropic Thermal Expansion of Hexagonal Boron Nitride in the 10−297.5 K Temperature Range. *Appl. Phys. A: Mater. Sci. Process.* **2002**, *75*, 431−435.
(50) Marini, A.; Garcia-Gonzalez, P.; Rubio, A. First-Principles Description of Correlation Effects in Layered Materials. *Phys. Rev. Lett.* **2006**, *96*, 136404.
(51) Kern, G.; Kresse, G.; Hafner, J. Ab Initio Calculation of the Lattice Dynamics and Phase Diagram of Boron Nitride. *Phys. Rev. B* **1999**, *59*, 8551.
(52) Pease, R. An X-Ray Study of Boron Nitride. *Acta Crystallogr.* **1952**, *5*, 356−361.
(53) Shi, Y.; Hamsen, C.; Jia, X.; Kim, K. K.; Reina, A.; Hofmann, M.; Hsu, A. L.; Zhang, K.; Li, H.; Juang, Z.-Y.; Dresselhaus, M. S.; Li, L.-J.; Kong, J. Synthesis of Few-Layer Hexagonal Boron Nitride Thin Film by Chemical Vapor Deposition. *Nano Lett.* **2010**, *10*, 4134−4139.
(54) Liu, L.; Feng, Y. P.; Shen, Z. X. Structural and Electronic Properties of h-BN. *Phys. Rev. B* **2003**, *68*, 104102.
(55) Mosuang, T. E.; Lowther, J. E. Relative stability of Cubic and Different Hexagonal Forms of Boron Nitride. *J. Phys. Chem. Solids* **2002**, *63*, 363−368.
(56) Yamamura, S.; Takata, M.; Sakata, M. Charge Density of Hexagonal Boron Nitride Using Synchrotron Radiation Powder Data by Maximum Entropy Method. *J. Phys. Chem. Solids* **1997**, *58*, 177−183.
(57) Catellani, A.; Posternak, M.; Baldereschi, A.; Freeman, A. J. Bulk and Surface Electronic Structure of Hexagonal Boron Nitride. *Phys. Rev. B* **1987**, *36*, 6105.
(58) Muramatsu, Y.; Kaneyoshi, T.; Gullikson, E. M.; Perera, R. C. C. Angle-Resolved Soft X-Ray Emission and Absorption Spectroscopy of Hexagonal Boron Nitride. *Spectrochim. Acta, Part A* **2003**, *59*, 1951−1957.
(59) Lomer, W. M.; Morton, K. W. The Electrostatic Energy of Boron Nitride. *Proc. Phys. Soc., Sect. A* **1953**, *66*, 772.
(60) Zunger, A.; Katzir, A.; Halperin, A. Optical Properties of Hexagonal Boron Nitride. *Phys. Rev. B* **1976**, *13*, 5560.
(61) Lennard-Jones, J. E.; Dent, B. M. Cohesion at a Crystal Surface. *Trans. Faraday Soc.* **1928**, *24*, 92−108.
(62) Natan, A.; Kronik, L.; Haick, H.; Tung, R. T. Electrostatic Properties of Ideal and Non-Ideal Polar Organic Monolayers: Implications for Electronic Devices. *Adv. Mater.* **2007**, *19*, 4103−4117.
(63) Borwein, D.; Borwein, J. M.; Taylor, K. F. Convergence of Lattice Sums and Madelung's Constant. *J. Math. Phys.* **1985**, *26*, 2999−3009.
(64) De Leeuw, S. W.; Perram, J. W. Electrostatic Lattice Sums for Semi-infinite Lattices. *Mol. Phys.* **1979**, *37*, 1313−1322.
(65) Zucker, I. J. Madelung Constants and Lattice Sums for Hexagonal Crystals. *J. Phys. A: Math. Gen.* **1991**, *24*, 873.
(66) Vernov, A.; Steele, W. A. The Electrostatic Field at a Graphite Surface and its Effect on Molecule-Solid Interactions. *Langmuir* **1992**, *8*, 155−159.
(67) Parry, D. E. The Electrostatic Potential in the Surface Region of an Ionic Crystal. *Surf. Sci.* **1975**, *49*, 433−440.
(68) Borwein, D.; Borwein, J. M.; Pinner, C. Convergence of Madelung-Like Lattice Sums. *Trans. Am. Math. Soc.* **1998**, *350*, 3131−3167.
(69) Fumi, F. G.; Tosi, M. P. Extension of the Madelung Method for the Evaluation of Lattice Sums. *Phys. Rev.* **1960**, *117*, 1466.
(70) Ewald, P. P. Die Berechnung Optischer und Elektrostatischer Gitterpotentiale. *Ann. Phys.* **1921**, *369*, 253−287.
(71) Toukmaji, A. Y.; Board, J. A. Ewald Summation Techniques in Perspective: a Survey. *Comput. Phys. Commun.* **1996**, *95*, 73−92.
(72) Hod, O.; Barone, V.; Scuseria, G. E. Half-Metallic Graphene Nanodots: A Comprehensive First-Principles Theoretical Study. *Phys. Rev. B* **2008**, *77*, 035411.
(73) Hod, O.; Peralta, J. E.; Scuseria, G. E. Edge Effects in Finite Elongated Graphene Nanoribbons. *Phys. Rev. B* **2007**, *76*, 233401.
(74) Fernandez-Rossier, J.; Palacios, J. J. Magnetism in Graphene Nanoislands. *Phys. Rev. Lett.* **2007**, *99*, 177204.
(75) Ezawa, M. Metallic Graphene Nanodisks: Electronic and Magnetic Properties. *Phys. Rev. B* **2007**, *76*, 245415.
(76) Shemella, P.; Zhang, Y.; Mailman, M.; Ajayan, P. M.; Nayak, S. K. Energy Gaps in Zero-Dimensional Graphene Nanoribbons. *Appl. Phys. Lett.* **2007**, *91*, 042101.
(77) Frisch, M. J.; Trucks, G. W.; Schlegel, H. B.; Scuseria, G. E.; Robb, M. A.; Cheeseman, J. R.; Scalmani, G.; Barone, V.; Mennucci, B.; Petersson, G. A.; Nakatsuji, H.; Caricato, M.; Li, X.; Hratchian, H. P.; Izmaylov, A. F.; Bloino, J.; Zheng, G.; Sonnenberg, J. L.; Hada, M.; Ehara, M.; Toyota, K.; Fukuda, R.; Hasegawa, J.; Ishida, M.; Nakajima, T.; Honda, Y.; Kitao, O.; Nakai, H.; Vreven, T.; Montgomery, J. A., Jr.; Peralta, J. E.; Ogliaro, F.; Bearpark, M.; Heyd, J. J.; Brothers, E.; Kudin, K. N.; Staroverov, V. N.; Kobayashi, R.; Normand, J.; Raghavachari, K.; Rendell, A.; Burant, J. C.; Iyengar, S. S.; Tomasi, J.; Cossi, M.; Rega, N.; Millam, N. J.; Klene, M.; Knox, J. E.; Cross, J. B.; Bakken, V.; Adamo, C.; Jaramillo, J.; Gomperts, R.; Stratmann, R. E.; Yazyev, O.; Austin, A. J.; Cammi, R.; Pomelli, C.; Ochterski, J. W.; Martin, R. L.; Morokuma, K.; Zakrzewski, V. G.; Voth, G. A.; Salvador, P.; Dannenberg, J. J.; Dapprich, S.; Daniels, A. D.; Farkas, Ö.; Foresman, J. B.; Ortiz, J. V.; Cioslowski, J.; Fox, D. J. *Gaussian 09*, Revision A.1; Gaussian, Inc.: Wallingford, CT, 2009.
(78) Hariharan, P. C.; Pople, J. A. The Influence of Polarization Functions on Molecular Orbital Hydrogenation Energies. *Theor. Chem. Acc.* **1973**, *28*, 213−222.
(79) Boys, S. F.; Bernardi, F. The Calculation of Small Molecular Interactions by the Differences of Separate Total Energies. Some Procedures with Reduced Errors. *Mol. Phys.* **1970**, *19*, 553−566.
(80) Simon, S.; Duran, M.; Dannenberg, J. J. How Does Basis Set Superposition Error Change the Potential Surfaces for Hydrogen-Bonded Dimers? *J. Chem. Phys.* **1996**, *105*, 11024−11031.

(81) The local density approximation is known to overbind systems which are not covalently bonded despite the lack of proper description of long-range correlation effects. Therefore, it is not considered in the present study.
(82) Perdew, J. P.; Burke, K.; Ernzerhof, M. Generalized Gradient Approximation Made Simple. *Phys. Rev. Lett.* **1996**, *77*, 3865.
(83) Becke, A. D. Density-Functional Thermochemistry. III. The Role of Exact Exchange. *J. Chem. Phys.* **1993**, *98*, 5648−5652.
(84) Zhao, Y.; Truhlar, D. G. Density Functionals with Broad Applicability in Chemistry. *Acc. Chem. Res.* **2008**, *41*, 157−167.
(85) Zhao, Y.; Truhlar, D. The M06 Suite of Density Functionals for Main Group Thermochemistry, Thermochemical Kinetics, Noncovalent Interactions, Excited States, and Transition Elements: Two New Functionals and Systematic Testing of Four M06-Class Functionals and 12 Other Functionals. *Theor. Chem. Acc.* **2008**, *120*, 215−241.
(86) Marom, N.; Tkatchenko, A.; Rossi, M.; Gobre, V. V.; Hod, O.; Scheffler, M.; Kronik, L. Dispersion Interactions with Density-Functional Theory: Benchmarking Semiempirical and Interatomic Pairwise Corrected Density Functionals. *J. Chem. Theory Comput.* **2011**, *7*, 3944−3951.
(87) Kganyago, K. R.; Ngoepe, P. E. Effects of Local and Gradient-Corrected Density Approximations on the Prediction of the Intralayer Lattice Distance c, in Graphite and LiC6. *Mol. Simul.* **1999**, *22*, 39−49.
(88) Here, care should be taken, as the Hartree term includes self-interaction. However, as we are discussing the interlayer part of the Hartree term, the self-repulsion contribution can be safely neglected as long as the density overlap between the two surfaces remains small.
(89) Ren, X.; Tkatchenko, A.; Rinke, P.; Scheffler, M. Beyond the Random-Phase Approximation for the Electron Correlation Energy: The Importance of Single Excitations. *Phys. Rev. Lett.* **2011**, *106*, 153003.
(90) Tkatchenko, A.; Scheffler, M. Accurate Molecular Van Der Waals Interactions from Ground-State Electron Density and Free-Atom Reference Data. *Phys. Rev. Lett.* **2009**, *102*, 073005.
(91) Marom, N.; Tkatchenko, A.; Scheffler, M.; Kronik, L. Describing Both Dispersion Interactions and Electronic Structure Using Density Functional Theory: The Case of Metal−Phthalocyanine Dimers. *J. Chem. Theory Comput.* **2009**, *6*, 81−90.
(92) Hirshfeld, F. L. Bonded-Atom Fragments for Describing Molecular Charge Densities. *Theor. Chem. Acc.* **1977**, *44*, 129−138.
(93) Chu, X.; Dalgarno, A. Linear Response Time-Dependent Density Functional Theory for van der Waals Coefficients. *J. Chem. Phys.* **2004**, *121*, 4083−4088.
(94) Tkatchenko, A. *Private communication*, 2011.
(95) Ding, X.; Ding, G.; Xie, X.; Huang, F.; Jiang, M. Direct Growth of Few Layer Graphene on Hexagonal Boron Nitride by Chemical Vapor Deposition. *Carbon* **2011**, *49*, 2522−2525.
(96) Fan, Y.; Zhao, M.; Wang, Z.; Zhang, X.; Zhang, H. Tunable Electronic Structures of Graphene/Boron Nitride Heterobilayers. *Appl. Phys. Lett.* **2011**, *98*, 083103−3.
(97) Giovannetti, G.; Khomyakov, P. A.; Brocks, G.; Kelly, P. J.; van den Brink, J. Substrate-Induced Band Gap in Graphene on Hexagonal Boron Nitride: Ab Initio Density Functional Calculations. *Phys. Rev. B* **2007**, *76*, 073103.
(98) Liu, Z.; Song, L.; Zhao, S.; Huang, J.; Ma, L.; Zhang, J.; Lou, J.; Ajayan, P. M. Direct Growth of Graphene/Hexagonal Boron Nitride Stacked Layers. *Nano Lett.* **2011**, *11*, 2032−2037.
(99) Slawinska, J.; Zasada, I.; Klusek, Z. Energy Gap Tuning in Graphene on Hexagonal Boron Nitride Bilayer System. *Phys. Rev. B* **2010**, *81*, 155433.
(100) Xue, J.; Sanchez-Yamagishi, J.; Bulmash, D.; Jacquod, P.; Deshpande, A.; Watanabe, K.; Taniguchi, T.; Jarillo-Herrero, P.; LeRoy, B. J. Scanning Tunnelling Microscopy and Spectroscopy of Ultra-Flat Graphene on Hexagonal Boron Nitride. *Nat. Mater.* **2011**, *10*, 282−285.
(101) Dean, C. R.; Young, A. F.; Meric, I.; Lee, C.; Wang, L.; Sorgenfrei, S.; Watanabe, K.; Taniguchi, T.; Kim, P.; Shepard, K. L.; Hone, J. Boron Nitride Substrates for High-Quality Graphene Electronics. *Nat. Nano.* **2010**, *5*, 722−726.
(102) Zobelli, A.; Ewels, C. P.; Gloter, A.; Seifert, G. Vacancy Migration in Hexagonal Boron Nitride. *Phys. Rev. B* **2007**, *75*, 094104.
(103) Chakarova-Kack, S. D.; Schroder, E.; Lundqvist, B. I.; Langreth, D. C. Application of van der Waals Density Functional to an Extended System: Adsorption of Benzene and Naphthalene on Graphite. *Phys. Rev. Lett.* **2006**, *96*, 146107.
(104) Zacharia, R.; Ulbricht, H.; Hertel, T. Interlayer Cohesive Energy of Graphite from Thermal Desorption of Polyaromatic Hydrocarbons. *Phys. Rev. B* **2004**, *69*, 155406.
(105) Girifalco, L. A.; Lad, R. A. Energy of Cohesion, Compressibility, and the Potential Energy Functions of the Graphite System. *J. Chem. Phys.* **1956**, *25*, 693−697.
(106) Benedict, L. X.; Chopra, N. G.; Cohen, M. L.; Zettl, A.; Louie, S. G.; Crespi, V. H. Microscopic Determination of the Interlayer Binding Energy in Graphite. *Chem. Phys. Lett.* **1998**, *286*, 490−496.
(107) Marom, N.; Tkatchenko, A.; Kapishnikov, S.; Kronik, L.; Leiserowitz, L. Structure and Formation of Synthetic Hemozoin: Insights From First-Principles Calculations. *Cryst. Growth Des.* **2011**, *11*, 3332−3341.

NOTE ADDED AFTER ASAP PUBLICATION

This article was published ASAP on February 24, 2012. The first paragraph in section II has been modified. The correct version was published on March 7, 2012.